Decadal warming events extended into central North America during the Last Glacial Period

Authors: C.J. Batchelor[1*], S.A. Marcott[1], I.J. Orland[2], F. He[3], R.L. Edwards[4]

[1]Department of Geoscience, University of Wisconsin-Madison, Madison, WI, USA.

[2]Wisconsin Geological and Natural History Survey, University of Wisconsin-Madison, Madison, WI, USA.

[3]Center for Climatic Research, Nelson Institute for Environmental Studies, University of Wisconsin-Madison, Madison, WI, USA.

[4]Department of Earth and Environmental Sciences, University of Minnesota, Minneapolis, MN, 55455, USA.

*Correspondence to: cambatch@mit.edu

Abstract: The connection between abrupt high-latitude warming during the Last Glacial Period – Dansgaard-Oeschger (DO) events– and rapid climate changes at lower latitudes has revealed inter-hemispheric teleconnections in the ocean-atmosphere system. Links between DO events and climate variability in mid-latitude, mid-continent settings remain, however, poorly understood, especially in North America where climate archives with sufficient time resolution are scarce. Here we examine a speleothem that grew from ~70-50 ka in Wisconsin (USA), and combine fluorescent imaging of its growth banding with an annual-resolution oxygen isotope ($\delta^{18}O$) record. Eight large (2.0-3.0‰) negative-$\delta^{18}O$ excursions, each with an onset in <10 annual growth bands, occur between 61-55 ka, when DO events 17-14 are recorded in the NGRIP ice core. Although the age model does not allow these $\delta^{18}O$ excursions to be matched to specific DO events, their magnitude and rapid onset support a credible link. Isotope-enabled climate simulations suggest that abrupt DO warming would increase the $\delta^{18}O$ of annual precipitation in the study area, and corroborate that warming of >10ºC in <10 years is thus required to produce the observed negative $\delta^{18}O$

excursions. Our findings of expansive abrupt DO warming in central North America has implications for environmental, climate, and ice sheet dynamics.

Dansgaard-Oeschger (DO) events[1] are a pervasive climate feature of the Last Glacial Period (~115-11 ka), and the rate and magnitude of these climatic events has been directly linked to ocean circulation of the North Atlantic[2]. Other abrupt climate changes outside of the high latitudes, including rapid changes in speleothem-derived records of oxygen isotopes ($\delta^{18}O$), have revealed an inter-hemispheric coupling between the North Atlantic and large-scale atmospheric circulation[3], such as changes in the position of the Intertropical Convergence Zone (ITCZ)[4]. The nature of these abrupt climate changes outside of the ITCZ and monsoon regions, however, is still largely an open question, specifically in regions such as the mid-continent of North America where the most dynamic ice sheet of the late Pleistocene once existed[5] and the impact of these abrupt climate changes on the ice sheet mass balance remains unknown[6].

Of the existing high-resolution climate reconstructions from North America, speleothem $\delta^{18}O$ records from the American southwest and west best capture a rapid regional climate response to DO Events in the last 60 ka. These records invoke a contemporaneous northward displacement of the polar jet stream during DO events that lead to decadal-scale increases in regional aridity[7–11]. These findings are consistent with other regional reconstructions on other continents that demonstrate a strong coupling between lower latitude climate changes associated with a shifting ITCZ position[4,12] or change in the regional monsoon with DO events[13,14].

As for continental interior locations, the few speleothem $\delta^{18}O$ records from the central and eastern United States report unremarkable changes during the Last Glacial Period[15–17] **(Figs. 1, 2)** that either cannot be tied to millennial-scale events or suggest small (<1‰) negative excursions during DO events. These results contrast with records from other continental interior locations that show rapid, notable climate changes in response to DO events[18,19]. One explanation for these muted proxy responses in mid-continental North America is that the $\delta^{18}O$ of seasonal moisture is

invariant and by extension temperature changes are negligible[15]. Large uncertainties remain regarding these interpretations, however, given the geographically sparse data from the mid-continents and whether decadal to centennial-scale climate changes can be fully resolved given the resolution of most mid-continental datasets during the Last Glacial Period.

Here we reconstruct climate changes from a 5.65 cm long speleothem collected from the mid-continent of North America in Cave of the Mounds (COM; 43.0°N, 89.8°W; 415 m a.s.l.; **Fig. 1**), which is uniquely positioned near the former margin of the Laurentide Ice Sheet[20]. Stalagmite "CM-5" (**Extended Data Fig. 1**) grew from 68-48 ka during the Last Glacial Period[21]. This record provides close insight into the magnitude and rate of climate changes adjacent to the southern margin of the ice sheet, and outside of the North American monsoon region[7–9].

Resolving a high-resolution speleothem climate record

Given the relatively slow growth rates of stalagmite CM-5, a combination of specialized imaging (confocal laser fluorescent microscopy, CLFM) and micro-scale analysis (secondary ion mass spectrometry, SIMS) were used to resolve a sub-annual- to annual-resolution $\delta^{18}O$ record across the sample (**Fig. 2)**. The presence of annually-laminated fluorescent growth bands[22] **(Fig. 3, Extended Data Fig. 2)** allow for interpretations of annual-resolution timeseries for the sections of the stalagmite where banding was visually coherent and uninterrupted by any growth hiatus. These bands range from 10-100s μm in thickness and by targeting high-precision SIMS $\delta^{18}O$ measurements in 10-μm spots across them we are able to reconstruct annual-resolution climatological signals. A total of 1,693 $\delta^{18}O$ measurements were completed along the central growth axis of stalagmite CM-5 (**Extended Data Fig. 3**) with $\delta^{18}O$ values ranging from -7.8 to -3.3‰ (VPDB; **Table S1**). Based on 12 U-Th ages that were previously measured along its central growth axis[21], the speleothem grew from 68 to 48 ka spanning the end of Marine Isotope Stage

(MIS) 4 and the beginning of MIS 3 during the last glacial period. Analytical uncertainty (2 s.d.) on the U-Th ages ranged from ±102 to ±1432 years, and the error envelope on the Bayesian age model of the timeseries ranged from ±520 to ±2802 years. We note that the five U-Th ages that span the growth period where abrupt $\delta^{18}O$ changes occur in our record (61-55 ka, *see* **Fig. 2** gray bar) have much lower analytical uncertainty than other U-Th ages that span the rest of the record. The 2 s.d. on the five U-Th ages that span 61-55 ka ranged from ±134 to ±192 years, and the error envelope on the Bayesian age model of the time series ranged from ±603 to ±667 years.

Millennial-scale climate variability

Overall, $\delta^{18}O$ values in CM-5 are higher during MIS 4 than MIS 3, and the isotope record largely resembles millennial-scale climate variability observed in both Greenland ice cores and Chinese monsoon records (**Fig. 2)**. A dominant feature in our $\delta^{18}O$ record is the presence of eight large-magnitude (2.0-3.0‰) negative-$\delta^{18}O$ excursions. According to the age model error, these negative $\delta^{18}O$ excursions occurred within a time window when several high-latitude DO events occurred in Greenland[23] (events 17-14; **Fig. 2)**. We clarify that we lack the age control to align our $\delta^{18}O$ excursions with the occurrence of specific DO events, however, we use annual band counting to provide physical evidence – similar to that of annually-layered ice cores – that each excursion has a rapid onset of 10 years or less. This finding supports a credible link between the occurrence of rapid $\delta^{18}O$ excursions at our field site from 61-55 ka and when DO events 17-14 are recorded in the NGRIP ice core[23] (**Fig. 2**).

The $\delta^{18}O$ of speleothem calcite reflects, in part, the $\delta^{18}O$ of cave dripwaters, which themselves represent a smoothed signal of rainfall $\delta^{18}O$ above the cave[24]. Thus, speleothem $\delta^{18}O$ records can respond to several climatic factors including changes in rainfall (amount, source),

and/or surface temperature[24]. The interaction of these climate factors, specifically in a mid-continental setting, complicates the interpretation of $\delta^{18}O$ variability in speleothems.

Climate model simulations

To help evaluate the most plausible factors driving the abrupt decreases of $\delta^{18}O$ in our record, the global rainfall isotopes were simulated for DO event 1/Greenland interstadial 1 (GI-1, Bølling warming[2,25,26]) based on the TraCE-21K simulation[27,28] between the late interval of Greenland Stadial 2 (GS-2, ~17.0 ka) to the peak of GI-1 (~14.5 ka[26]) (Methods and Supplementary **Table S5**). These simulations of DO event 1 were used as their climate states are analogous to other DO events during Last Glacial Period[2], with stronger AMOC and higher atmospheric CO_2 and CH_4 during the peaks of DO events (Greenland interstadials) and weaker AMOC and lower CO_2 and CH_4 during the Greenland Stadials prior to the DO events[29–32]. One isotope simulation was run with boundary conditions from the peak of GS-1 in TraCE-21K to simulate global rainfall isotopes during the peaks of DO events, and another with boundary conditions derived from the late interval of GS-2 to simulate global rainfall isotopes during the stadial condition prior to the peaks of DO events. Thus, the differences of simulated global rainfall isotopes from the two simulations provide the best opportunity to evaluate the most plausible factors driving the abrupt decreases of $\delta^{18}O$ in our record in response to the DO events during the Last Glacial Period. The monthly climatology of surface temperature, precipitation rate, and precipitation $\delta^{18}O$ from each simulation were collected from the COM regional grid cell (43ºN, 90ºW) (**Fig. 4a-c)**. Comparing the monthly data between the two simulations (**Fig. 4d-f)** highlights key differences between the two climate states that were used in our interpretation of the CM-5 speleothem $\delta^{18}O$ record.

The climate simulations (**Fig. 4**, **Table S3)** suggest there was an overall increase in annual precipitation at COM during abrupt warming events of the Last Glacial Period, mostly related to an increase in summer precipitation (**Fig. 4b, Extended Data Fig. 4**). The annual amount-weighted $\delta^{18}O$ of precipitation during the peak of DO warm period is simulated to increase by 2.1‰ versus the stadial condition prior to the DO events (**Fig. 4c)**. The elevated $\delta^{18}O$ is likely explained by an increase in the amount of higher-$\delta^{18}O$ precipitation delivered to the mid-continent from Eastern Tropical Pacific and Gulf of Mexico[33,34]. Notably, this mechanism has been identified in other climate reconstructions of DO events in North America[7,8,15]. We therefore conclude that rainfall $\delta^{18}O$ over COM likely increased during DO events, leaving another climatic factor responsible for the rapid 2.0-3.0‰ decreases in the CM-5 $\delta^{18}O$ record (**Fig. 2, 3)**.

Decadal warming events

Temperature affects the $\delta^{18}O$ of speleothem calcite during fractionation by a known relationship of -0.18 to -0.24‰/ºC[35]. Thus, increases in annual temperature inside COM could explain the decreasing excursions in the CM-5 record. On average, $\delta^{18}O$ excursions of 2.5‰ (2.0-3.0‰) were likely caused by temperature increases of >10ºC based on the temperature fractionation effects of -0.18 to -0.24‰/ºC[35]. We note, however, that the actual magnitude of temperature change is likely to be larger than 10ºC due to the counteracting effect of increased rainfall $\delta^{18}O$ that originated from tropical regions as suggested by the model simulation (**Fig. 4c**). This increase of mean annual surface temperature in mid-continent North America during DO events is consistent in magnitude with warming at much higher latitudes[36]. Further corroborating this interpretation, the modeled annual warming at COM amounts to 8-10ºC for DO event 1 (**Fig. 1 and 4d**, **Table S3, Extended Data Fig. 5)** and is attributed to the superposition of climatic

responses to the abrupt AMOC recovery and the increase of atmospheric CO_2 during DO event 1[27].

Rapid, ~10°C warming at COM during DO events is consistent with North American[37], southern European and Mediterranean pollen reconstructions[19,38], which demonstrate millennial-scale vegetation changes during the Last Glacial Period likely driven by sharp temperature swings. Our study highlights, however, that the magnitude of temperature change in the region of COM during DO events was likely greater than previously interpreted.

Furthermore, the fluorescent growth banding in the sample provides an unprecedented level of temporal resolution across these warming events and establishes that their full magnitude occurred within a decade (**Fig. 3**). Outside of a few records[39,40], this is a first look at a record that both corroborates the magnitude of temperature change and provides direct evidence for the subdecadal rate of change. We propose that other speleothem records in central and eastern United States that record muted (<1‰) millennial-scale $\delta^{18}O$ shifts during the Last Glacial Period do so for a number of plausible reasons, including: the comparatively low temporal resolution of drill-sampling methods, their proximity to an oceanic moisture source and thus reduced Rayleigh distillation, or perhaps because of the counteracting effects of different regional moisture source changes and temperature on their isotopic signals.

The ability to resolve high-magnitude, abrupt climate changes in the CM-5 record provides the evidence that warmings of >10°C occurred in mid-continental North America over a time span of decades or less during the last glacial period. This finding shows that temperatures outside of Greenland also warmed abruptly during DO events[41], and implies that the underlying processes driving these changes occurred on similar timescales and were rapidly propagated to the continental interior of North America. These findings have important implications when

considering how widespread and quickly warming spread in the Northern Hemisphere during DO events – especially across a large ice sheet and into continental interiors – and how dynamically the climate system can react on human timescales.

Acknowledgments

This work was supported by the U.S. National Science Foundation (NSF) (grant P2C2-1805629 to S. M. and I. O.), the WiscSIMS Laboratory which is supported by the NSF (grants EAR-1355590, EAR-1658823), the University of Wisconsin-Madison Office of the Vice Chancellor for Research and Graduate Education with funding from the Wisconsin Alumni Research Foundation (F.H.), and the Isotope Laboratory at the University of Minnesota (R. L. E.). This research used resources of the Oak Ridge Leadership Computing Facility at the Oak Ridge National Laboratory, which is supported by the Office of Science of the US Department of Energy under contract number DE-AC05-00OR22725 (F.H.). We thank J. Klimczak and A. Wescott for their permission to collect stalagmite samples at Cave of the Mounds, Rich Slaughter for sample collection help, Drae Rogers for sample preparation, Lance Rodenkirch for CLFM help at the University of Wisconsin–Madison Optical Imaging Core, and Lawrence R. Edwards and associated colleagues for prior U-Th analyses at the University of Minnesota. Stalagmite CM-5 is curated at the University of Wisconsin–Madison Geology Museum.

Author contribution statement

C.J.B. performed all sample analyses and sample processing, and with S.M. and I.J.O conceptualize the project and acquired the funding for sample collection and oxygen isotope analysis for the project. R.L.E. provided funding and support for the geochronology of samples,

which C.J.B. performed geochronological lab work on samples at University of Minnesota. F.H. performed the climate model simulation and contributed to the interpretation of oxygen isotope excursions. C.J.B., S.A.M., and I.J.O wrote the original draft, and all authors participated in the final writing and editing of the manuscript.

Competing interests

The authors declare no competing interests.

Figure 1. North American speleothem $\delta^{18}O$ records from the last glacial period and their corresponding magnitude of $\delta^{18}O$ change that occurred during a time of Dansgaard Oeschger (DO) events in Greenland. The location of Cave of the Mounds (this study) is shown, as well as all other North American speleothem records that show distinct $\delta^{18}O$ changes during DO Events with their corresponding reference number in the bottom right[7-11,15-17]. Note the magnitude of $\delta^{18}O$ change during DO Events is scaled to the size of the sample location dot. The MIS 4 Laurentide Ice Sheet approximate extent is shown[20]. The base map was plotted from the R package 'maps' from Brownrigg et al., (2022) and is overlain with the modeled warming during DO events (the simulated difference between Greenland Interstadial event 1, GI-1, and Greenland Stadial event 2, GS-2).

Figure 2. Stalagmite CM-5 $\delta^{18}O$ record in comparison to other regional $\delta^{18}O$ records of the last-glacial period. a, Cave of the Mounds (COM; this study) $\delta^{18}O$ record (black line with 2 standard deviation analytical error shown by gray envelope), with associated U-Th ages (black dots with 2 standard deviation error bars). Data are presented as mean values +/- standard deviation. Note the error of our age model ranged from 520 to 2800 years and was on average 730

years. **b**, A stalagmite $\delta^{18}O$ record from Buckeye Creek Cave, WV[15] (red line) showing relatively low-magnitude $\delta^{18}O$ changes during the last glacial period. **c**, A compilation of Chinese speleothem $\delta^{18}O$ records[12] (orange line), showing high-magnitude $\delta^{18}O$ changes, which reflects the sensitivity of the East Asian monsoon system to high-latitude warmings (DO events) during the last glacial period. Note the scale of the y-axis in panels A-C are the same to allow for one-to-one comparison. **d**, The North Greenland Ice Sheet Project (NGRIP) $\delta^{18}O$ record[23] (blue line), showing the timing of abrupt warming DO Events (labeled #s). The gray shaded bar corresponds to the panels in **Fig. 3**.

Figure 3. The timing and rate of negative $\delta^{18}O$ excursions in the CM-5 stalagmite record. CLFM images of fluorescent banding in stalagmite CM-5 (top panels), and the corresponding $\delta^{18}O$ record of CM-5 (bottom panel, black line) where $\delta^{18}O$ negative excursions are identified (gray shading). The age scale is based on U-Th ages that ranged from ±102 to ±1432 years, and the error envelope on the Bayesian age model of the timeseries ranged from ±520 to ±2802 years, thus the relative ages are precise, but the absolute ages are uncertain. The magnitude (‰) and distance (μm) of each rapid $\delta^{18}O$ excursion is also labeled, as well as where in the sample $\delta^{18}O$ measurements were made (dashed white lines). The zoomed-in images show the number of bright-to-dark fluorescent band couplets (*1 "band"*=1 year) each sharp $\delta^{18}O$ excursion occurs in, which is consistently 10 bands or less. For scale, in the zoomed-in images, the black ovals (outlined in white) are the 10-μm diameter $\delta^{18}O$ measurements by SIMS.

Figure 4. Modeled monthly climate data from two isotope-enabled climate model simulations of analogous DO conditions. **a-c**, Modeled values of surface temperature (ºC), precipitation rate (mm/month) and precipitation $\delta^{18}O$ values (‰) for two climate model simulations. One was run

to reflect abrupt warm conditions during DO Events (GI-1; red solid line), and another was run to reflect background mean glacial state conditions (GS-2; blue solid line). Note the precipitation-weighted annual $\delta^{18}O$ for each simulation is shown in panel (**c**) (dashed lines), demonstrating the +2.11‰ difference from GI-1 to GS-2. **d-f**, Differences between the warm (GI-1) and cold (GS-2) simulation show how surface temperature (**d**) and rainfall (**e**) potentially changed precipitation $\delta^{18}O$ (**f**) during abrupt DO Events. Raw data used to make this graph can be found in **Supplementary Table S3.**

References

1. Dansgaard, W. *et al.* North Atlantic climatic oscillations revealed by deep Greenland ice cores. *Climate processes and climate sensitivity* 288–298 (1984).
2. Clement, A. C. & Peterson, L. C. Mechanisms of abrupt climate change of the last glacial period. *Reviews of Geophysics* **46**, (2008).
3. Corrick, E. C. *et al.* Synchronous timing of abrupt climate changes during the last glacial period. *Science* **369**, 963–969 (2020).
4. Wang, Y.-J. *et al.* A high-resolution absolute-dated late Pleistocene monsoon record from Hulu Cave, China. *Science* **294**, 2345–2348 (2001).
5. Clark, J. A. The reconstruction of the Laurentide Ice Sheet of North America from sea level data: Method and preliminary results. *Journal of Geophysical Research: Solid Earth* **85**, 4307–4323 (1980).
6. Gregoire, L. J., Otto-Bliesner, B., Valdes, P. J. & Ivanovic, R. Abrupt Bølling warming and ice saddle collapse contributions to the Meltwater Pulse 1a rapid sea level rise. *Geophysical research letters* **43**, 9130–9137 (2016).

7. Asmerom, Y., Polyak, V. J. & Burns, S. J. Variable winter moisture in the southwestern United States linked to rapid glacial climate shifts. *Nature Geoscience* **3**, 114 (2010).
8. Wagner, J. D. *et al.* Moisture variability in the southwestern United States linked to abrupt glacial climate change. *Nature Geoscience* **3**, 110–113 (2010).
9. Oster, J. L. *et al.* Millennial-scale variations in western Sierra Nevada precipitation during the last glacial cycle MIS 4/3 transition. *Quaternary Research* **82**, 236–248 (2014).
10. Lachniet, M. S., Denniston, R. F., Asmerom, Y. & Polyak, V. J. Orbital control of western North America atmospheric circulation and climate over two glacial cycles. *Nature communications* **5**, 1–8 (2014).
11. Oster, J. L., Weisman, I. E. & Sharp, W. D. Multi-proxy stalagmite records from northern California reveal dynamic patterns of regional hydroclimate over the last glacial cycle. *Quaternary Science Reviews* **241**, 106411 (2020).
12. Cheng, H. *et al.* The Asian monsoon over the past 640,000 years and ice age terminations. *nature* **534**, 640–646 (2016).
13. Burns, S. J., Fleitmann, D., Matter, A., Kramers, J. & Al-Subbary, A. A. Indian Ocean climate and an absolute chronology over Dansgaard/Oeschger events 9 to 13. *Science* **301**, 1365–1367 (2003).
14. Cai, Y. *et al.* High-resolution absolute-dated Indian Monsoon record between 53 and 36 ka from Xiaobailong Cave, southwestern China. *Geology* **34**, 621–624 (2006).
15. Cheng, H. *et al.* Eastern North American climate in phase with fall insolation throughout the last three glacial-interglacial cycles. *Earth and Planetary Science Letters* **522**, 125–134 (2019).

16. Nissen, J. High-resolution speleothem record of climate variability during the late Pleistocene from Spring Valley Caverns, Minnesota. (2018).
17. Dorale, J. A., Edwards, R. L., Ito, E. & González, L. A. Climate and vegetation history of the midcontinent from 75 to 25 ka: a speleothem record from Crevice Cave, Missouri, USA. *Science* **282**, 1871–1874 (1998).
18. Cheng, H. *et al.* The climatic cyclicity in semiarid-arid central Asia over the past 500,000 years. *Geophysical Research Letters* **39**, (2012).
19. Genty, D. *et al.* Precise dating of Dansgaard–Oeschger climate oscillations in western Europe from stalagmite data. *Nature* **421**, 833–837 (2003).
20. Gowan, E. J. *et al.* A new global ice sheet reconstruction for the past 80 000 years. *Nature communications* **12**, 1–9 (2021).
21. Batchelor, C. J. *et al.* Distinct Permafrost Conditions Across the Last Two Glacial Periods in Midlatitude North America. *Geophysical Research Letters* **46**, 13318–13326 (2019).
22. Batchelor, C. J., Marcott, S. A., Orland, I. J. & Kitajima, K. Late Holocene increase of winter precipitation in mid-continental North America from a seasonally resolved speleothem record. *Geology* (2022).
23. NGRIP members. High-resolution record of Northern Hemisphere climate extending into the last interglacial period. *Nature* **431**, 147 (2004).
24. Lachniet, M. S. Climatic and environmental controls on speleothem oxygen-isotope values. *Quaternary Science Reviews* **28**, 412–432 (2009).
25. Dansgaard, W. *et al.* Evidence for general instability of past climate from a 250-kyr ice-core record. *Nature* **364**, 218–220 (1993).

26. Rasmussen, S. O. *et al.* A stratigraphic framework for abrupt climatic changes during the Last Glacial period based on three synchronized Greenland ice-core records: refining and extending the INTIMATE event stratigraphy. *Quaternary Science Reviews* **106**, 14–28 (2014).

27. Liu, Z. *et al.* Transient simulation of last deglaciation with a new mechanism for Bølling-Allerød warming. *Science* **325**, 310–314 (2009).

28. He, F. *Simulating transient climate evolution of the last deglaciation with CCSM 3*. vol. 72 (2011).

29. Blunier, T. & Brook, E. J. Timing of millennial-scale climate change in Antarctica and Greenland during the last glacial period. *Science* **291**, 109–112 (2001).

30. McManus, J. F., Francois, R., Gherardi, J.-M., Keigwin, L. D. & Brown-Leger, S. Collapse and rapid resumption of Atlantic meridional circulation linked to deglacial climate changes. *Nature* **428**, 834–837 (2004).

31. Ahn, J. & Brook, E. J. Atmospheric CO2 and climate on millennial time scales during the last glacial period. *science* **322**, 83–85 (2008).

32. Henry, L. G. *et al.* North Atlantic ocean circulation and abrupt climate change during the last glaciation. *Science* **353**, 470–474 (2016).

33. Simpkins, W. W. Isotopic composition of precipitation in central Iowa. *Journal of Hydrology* **172**, 185–207 (1995).

34. Bryson, R. A. & Hare, F. K. *Climates of North America*. vol. 11 (Elsevier New York, 1974).

35. Kim, S.-T. & O'Neil, J. R. Equilibrium and nonequilibrium oxygen isotope effects in synthetic carbonates. *Geochimica et cosmochimica acta* **61**, 3461–3475 (1997).

36. Severinghaus, J. P. & Brook, E. J. Abrupt climate change at the end of the last glacial period inferred from trapped air in polar ice. *Science* **286**, 930–934 (1999).

37. Jimenez-Moreno, G. *et al.* Millennial-scale variability during the last glacial in vegetation records from North America. *Quaternary Science Reviews* **29**, 2865–2881 (2010).

38. Allen, J. R. *et al.* Rapid environmental changes in southern Europe during the last glacial period. *Nature* **400**, 740–743 (1999).

39. Hughen, K. A., Overpeck, J. T., Peterson, L. C. & Trumbore, S. Rapid climate changes in the tropical Atlantic region during the last deglaciation. *Nature* **380**, 51–54 (1996).

40. Deplazes, G. *et al.* Links between tropical rainfall and North Atlantic climate during the last glacial period. *Nature Geoscience* **6**, 213–217 (2013).

41. Steffensen, J. P. *et al.* High-resolution Greenland ice core data show abrupt climate change happens in few years. *Science* **321**, 680–684 (2008).

Methods

Seasonal fluorescent bands

Speleothems can form fluorescent growth bands as a result of groundwater flushing organic acids from the overlying soil into the cave, eventually coprecipitating in speleothem calcite[42]. Former studies have suggested the occurrence of fluorescence in speleothem samples are a result of seasonal variability of organic acids in cave drip waters[42-47]. This seasonal signal is a result of climate-driven changes in the input of organic substances into cave drip waters. Fluorescent growth bands in COM speleothems are preserved as couplets of bright (high fluorescence, interpreted as relatively high organic acid content) and dark (non-fluorescent, interpreted as

relatively low organic acid content) bands. These couplets typically range in thickness from 10-200μm. We interpret one bright-to-dark couplet to represent one annual cycle.

To quantify the amount of time each sharp negative $\delta^{18}O$ excursion occurred in within the CM-5 record, we identified where in the sample these $\delta^{18}O$ changes occurred and visually counted the number of bright-to-dark fluorescent band couplets ("*1 band*") that spanned the sharp onset of the excursion. This visual inspection revealed that each sharp $\delta^{18}O$ decrease happened in 10 bands or less (**Fig. 3**), thus often within a decade.

Sample preparation, confocal laser fluorescent microscopy. To prepare stalagmite sample CM-5 for SIMS analysis, a thin, 5-mm wide slab was cut along the entire length of the central growth axis. This thin slab was then cut into four separate ~15 x 3 mm sized chips that were cast, along with 5 grains of UWC-3[48] (calcite standard; $\delta^{18}O$ of -12.49‰ VSMOW) for each mount, into two 2.5-cm-diamter epoxy rounds with two chips in each round. The epoxy rounds were ground flat with a fixed diamond-pad and then polished with 6, 3, and 1 μm diamond suspensions on a lapping wheel. A final polish of 0.05 μm was applied with a colloidal alumina solution, followed immediately by a gentle rinse by water and drying by air blast. These two sample epoxy rounds were then cleaned with soap and dried with air, then imaged both on the optical microscope and confocal laser fluorescent microscope (CLFM) at the University of Wisconsin-Madison. The CLFM imaging was completed at the Optical Imaging Core at the Wisconsin Institutes for Medical Research using a Nikon A1RS HD Confocal Microscope with a 488-nm-wavelength excitation laser. Images of speleothem fluorescence were collected using an emission filter that allows light with wavelengths between 505 and 539 nm (visible, green), and linear image adjustments were applied to increase the contrast and brightness of published images.

SIMS $\delta^{18}O$ analysis, QGIS, and the age-depth model. Oxygen isotope data in speleothem CM-5 were analyzed in the WiscSIMS lab at the University of Wisconsin-Madison using a CAMECA IMS 1280 large radius multicollector ion microprobe—the Secondary Ion Mass Spectrometer (SIMS). A total of 1,760 10-μm-diameter SIMS $\delta^{18}O$ analyses were collected across all four sample chips of CM-5 during four separate analysis sessions (**Table S1**). Broadly, these measurements were made by spacing $\delta^{18}O$ measurements every 50-μm, though sections of the speleothem were sampled at higher resolution (10-μm spacing) to target individual growth bands. A sampling "bracket" method, consisting of four standard UWC-3 calcite measurements made every 20-25 sample analyses measurements, was also implemented to calculate the associated standard deviation (2SD) error for each analysis point. To assess quality control of the collected SIMS $\delta^{18}O$ data, two metrics were monitored. The first metric is the relative yield (% units, Table S1), which is the yield ($^{16}O^-$ cps/primary beam intensity) of each sample analysis divided by the average yield of the bracketing standards. The second metric is the background-corrected OH/O ratio (**Table S1**), which has been interpreted by earlier studies[49,50] to be a qualitative measure of water and/or organic content in low-temperature carbonates. Once these metrics were calculated, outliers were identified statistically by using a Tukey outlier definition[51], and those outliers (n=67) were removed from further consideration in the manuscript. As such, the final SIMS $\delta^{18}O$ record of CM5 consisted of 1,693 analyses and had an average sampling resolution of 25 μm/analysis.

An open-source geographic information system software, QGIS, was used to generate a microspatial database of sample CM-5 to produce an accurate age-depth model between already-measured U-Th ages[21] and SIMS $\delta^{18}O$ analyses **(Extended Data Fig. 3, Table S2)**. Prior work[52,53] at the WiscSIMS lab established the guidelines used for constructing the microspatial database for this study. The age model used was a Bayesian model for sedimentary deposition, specifically

OxCal 4.4[54], with a static k-value of 0.1[54]. The resulting age model revealed relatively linear growth of sample CM-5 (**Extended Data Fig. 1)** with no visual evidence for prolonged growth hiatuses or dissolution, except for a hiatus at ~44k that is evident from an unconformity in the fluorescent banding (**Extended Data Fig. 1-2).**

Climate model simulations

Rainfall isotope simulations. We performed the global rainfall isotope simulations for DO event 1 between GS-1 and GS-2 with isotope-enabled Community Atmosphere Model version 3 (isoCAM3)[55]. The isoCAM3 model incorporates stable water isotopes into CAM3 with fractionation associated with surface evaporation and cloud processes. We ran the isotope-enabled isoCAM3 atmosphere model with boundary conditions at 14.4ka for GS-1 and 17.0ka for GS-2 from the TraCE-21K simulation, a transient simulation of the past 21,000 years forced by Earth's orbital variations, greenhouse gases, ice-sheet variations, and FW forcing[27,28]. Previous studies have demonstrate that the TraCE-21K simulation exhibit reasonable agreements with the data reconstructions of transient evolution of surface temperature over Greenland, sea surface temperature from both Northern and Southern Hemisphere and tropical rainfall between GS-2 to the peak of GI-1[27,56–58]. We note there are variations of the sizes of Northern Hemisphere ice sheets between DO event 1 and other DO events, but the uncertainties of ice sheet reconstructions during the last glacial period prevent us from making definitive investigations. We used the same preindustrial surface ocean $\delta^{18}O$ values in both GS-1 and GS-2 isoCAM3 simulations to isolate the fractionation associated with atmospheric processes. Each experiment is forced by a 50-year history of monthly sea surface temperature and sea ice from the deglaciation experiment. Ocean water $\delta^{18}O$ in this model does not respond to runoff or meteoric water. Computational resources were provided by the Cheyenne: HPE/SGI ICE XA System (University Community Computing)[59].

To demonstrate the feasibility and sensitivity of our interpretation given the magnitude of rainfall $\delta^{18}O$ change suggested by the climate model, we ran the ISOLUTION proxy-system model[60], using reasonable estimates of cave conditions and a conservative range of rainfall $\delta^{18}O$ values, to model relative changes in calcite $\delta^{18}O$ at the magnitude we observe. Results support our interpretation and are reported in the Supplementary Information (**Extended Data Table 6**).

Data availability

The data that support the findings of this study are available in the NOAA paleoclimate database: https://www.ncei.noaa.gov/products/paleoclimatology.

References

42. McGarry, S. F. & Baker, A. Organic acid fluorescence: applications to speleothem palaeoenvironmental reconstruction. *Quaternary Science Reviews* **19**, 1087–1101 (2000).

43. Senesi, N., Miano, T. M., Provenzano, M. R. & Brunetti, G. Characterization, differentiation, and classification of humic substances by fluorescence spectroscopy. *Soil Science* **152**, 259–271 (1991).

44. Baker, D. G. & Keuhnast, E. L. Part X: Precipitation Normals for Minnesota: 1941-1970. *Climate of Minnesota* (1978).

45. Tan, M. *et al.* Applications of stalagmite laminae to paleoclimate reconstructions: comparison with dendrochronology/climatology. *Quaternary Science Reviews* **25**, 2103–2117 (2006).

46. Orland, I. J. *et al.* Climate deterioration in the Eastern Mediterranean as revealed by ion microprobe analysis of a speleothem that grew from 2.2 to 0.9 ka in Soreq Cave, Israel.

Quaternary Research **71**, 27–35 (2009).

47. Orland, I. J. *et al.* Resolving seasonal rainfall changes in the Middle East during the last interglacial period. *Proceedings of the National Academy of Sciences* **116**, 24985–24990 (2019).

48. Kozdon, R., Ushikubo, T., Kita, N. T., Spicuzza, M. & Valley, J. W. Intratest oxygen isotope variability in the planktonic foraminifer N. pachyderma: Real vs. apparent vital effects by ion microprobe. *Chemical Geology* **258**, 327–337 (2009).

49. Orland, I. J. *et al.* Direct measurements of deglacial monsoon strength in a Chinese stalagmite. *Geology* **43**, 555–558 (2015).

50. Wycech, J. B. *et al.* Comparison of δ18O analyses on individual planktic foraminifer (Orbulina universa) shells by SIMS and gas-source mass spectrometry. *Chemical Geology* **483**, 119–130 (2018).

51. Tukey, J. *Exploratory Data Analysis*. (Addison-Wesley Publishing Co., Reading, 1977).

52. Linzmeier, B. J., Kitajima, K., Denny, A. C. & Cammack, J. N. *Making maps on a micrometer scale, Eos, 99*. (2018).

53. QGIS Development Team. QGIS Geographic Information System. (2019).

54. Ramsey, C. B. & Lee, S. Recent and planned developments of the program OxCal. *Radiocarbon* **55**, 720–730 (2013).

55. Noone, D. & Sturm, C. Comprehensive dynamical models of global and regional water isotope distributions. in *Isoscapes* 195–219 (Springer, 2010).

56. He, F. *et al.* Northern Hemisphere forcing of Southern Hemisphere climate during the last deglaciation. *Nature* **494**, 81–85 (2013).

57. Buizert, C. *et al.* Greenland temperature response to climate forcing during the last

deglaciation. *Science* **345**, 1177–1180 (2014).

58. He, F. & Clark, P.U., Freshwater forcing of the Atlantic meridional overturning circulation revisited. *Nature Climate Change,* **12,** 449-454 (2022).

59. Computational Information Systems Laboratory, National Center for Atmospheric Research, 2019: https://doi.org/10.6065/D6RX99HX.

60. Deininger, Michael, and Denis Scholz. "ISOLUTION 1.0: an isotope evolution model describing the stable oxygen ($\delta^{18}O$) and carbon ($\delta^{13}C$) isotope values of speleothems." *International Journal of Speleology* 48.1 (2019): 3.

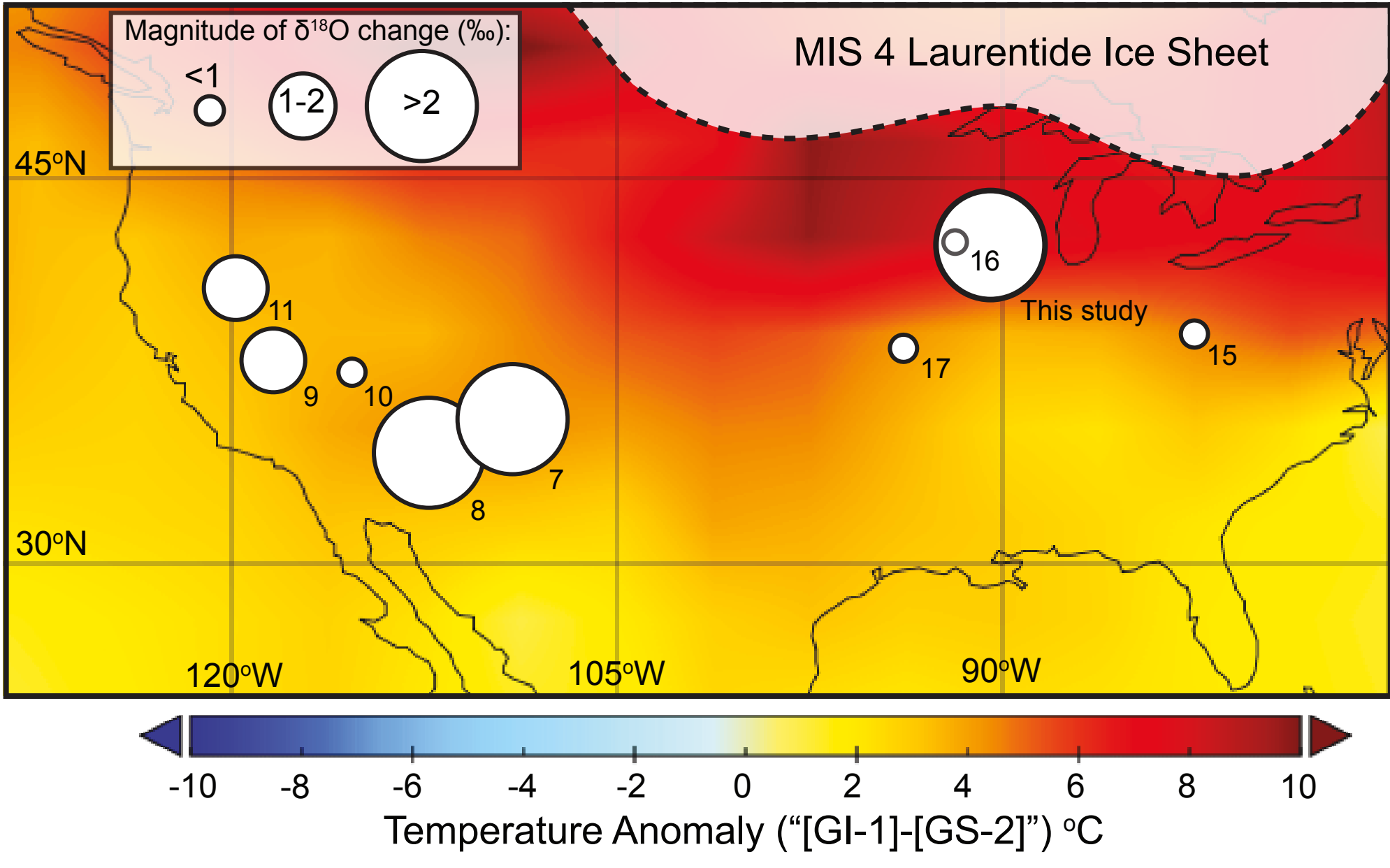
Magnitude of δ18O change (‰):
<1
1-2
>2
MIS 4 Laurentide Ice Sheet
45°N
30°N
120°W
105°W
90°W
16
This study
17
15
11
9
10
8
7
-10
-8
-6
-4
-2
0
2
4
6
8
10
Temperature Anomaly ("[GI-1]-[GS-2]") °C

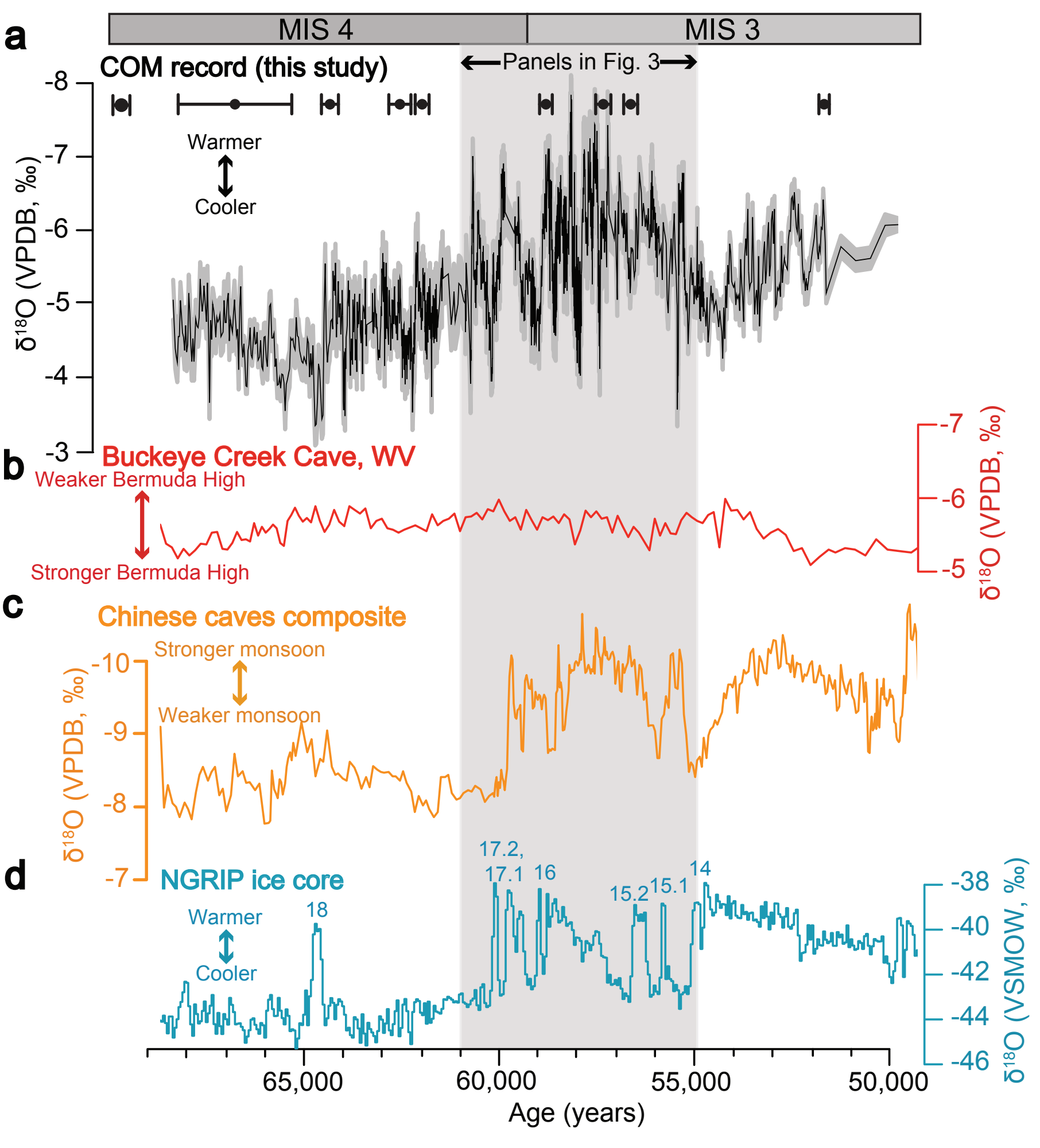
a
MIS 4
MIS 3
COM record (this study)
Panels in Fig. 3
Warmer
Cooler
δ18O (VPDB, ‰)
-8
-7
-6
-5
-4
-3
b
Buckeye Creek Cave, WV
Weaker Bermuda High
Stronger Bermuda High
-7
-6
-5
δ18O (VPDB, ‰)
c
Chinese caves composite
Stronger monsoon
Weaker monsoon
δ18O (VPDB, ‰)
-10
-9
-8
-7
d
NGRIP ice core
Warmer
Cooler
18
17.2,
17.1
16
15.2
15.1
14
-38
-40
-42
-44
-46
δ18O (VSMOW, ‰)
65,000
60,000
55,000
50,000
Age (years)

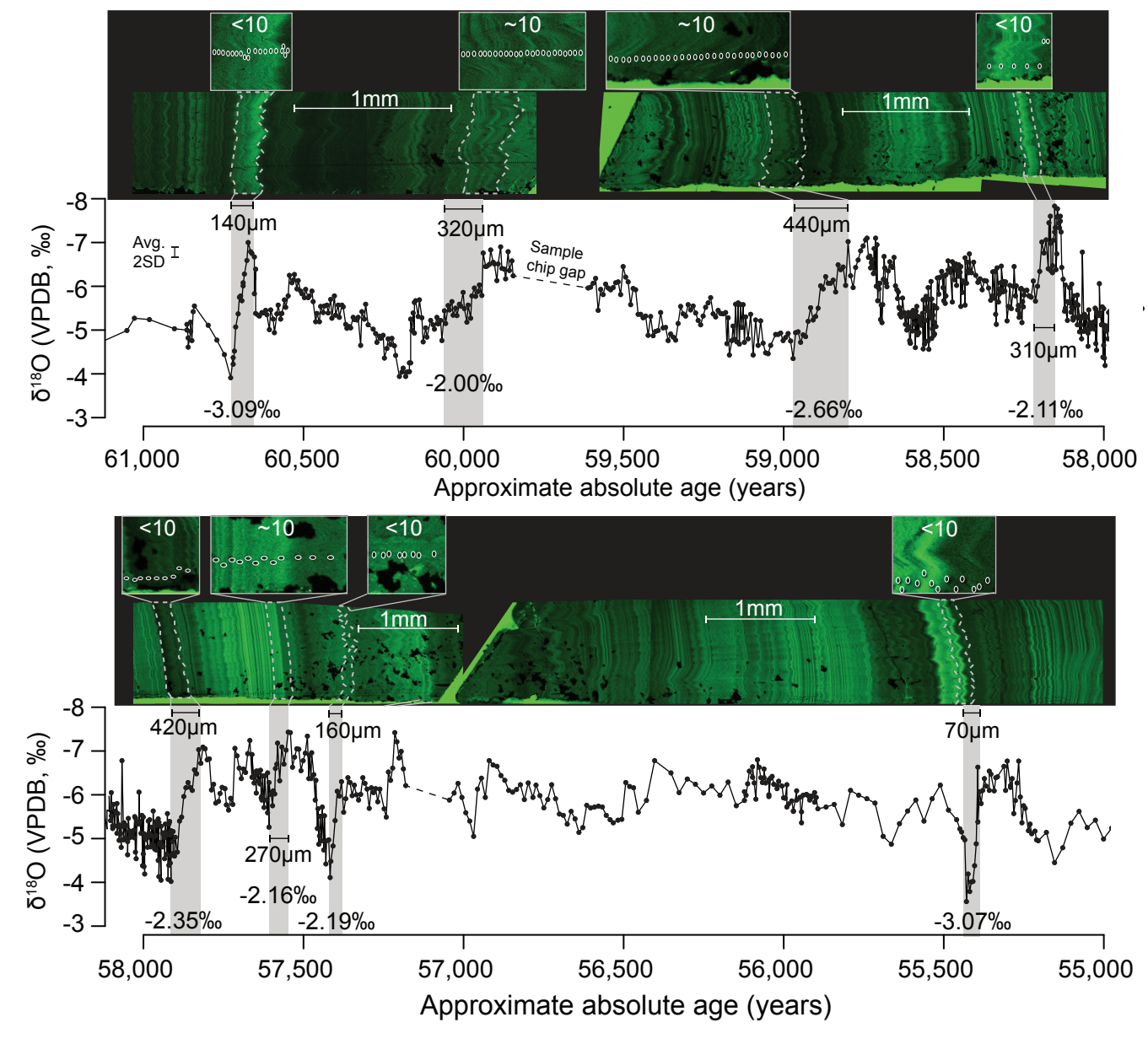
<10
~10
~10
<10
1mm
1mm
140µm
320µm
440µm
310µm
Avg. 2SD
Sample chip gap
-3.09‰
-2.00‰
-2.66‰
-2.11‰
δ18O (VPDB, ‰)
-8
-7
-6
-5
-4
-3
61,000
60,500
60,000
59,500
59,000
58,500
58,000
Approximate absolute age (years)
<10
~10
<10
<10
1mm
1mm
420µm
160µm
70µm
270µm
-2.16‰
-2.35‰
-2.19‰
-3.07‰
δ18O (VPDB, ‰)
-8
-7
-6
-5
-4
-3
58,000
57,500
57,000
56,500
56,000
55,500
55,000
Approximate absolute age (years)

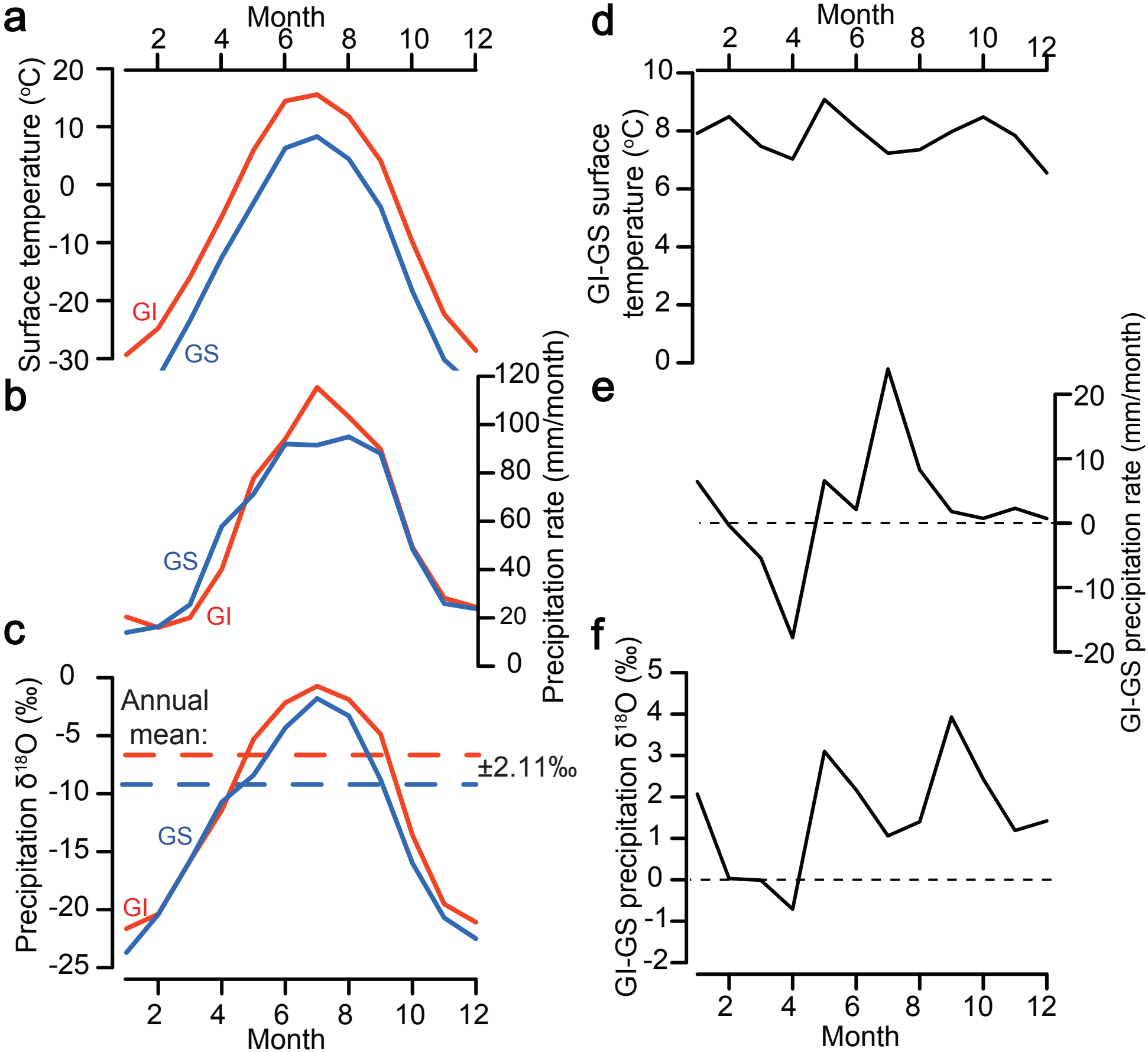
a
Month
2
4
6
8
10
12
Surface temperature (°C)
20
10
0
-10
-20
-30
GI
GS
b
120
100
80
60
40
20
0
Precipitation rate (mm/month)
GS
GI
c
Precipitation δ18O (‰)
0
-5
-10
-15
-20
-25
Annual mean:
±2.11‰
GS
GI
Month
d
Month
GI-GS surface temperature (°C)
10
8
6
4
2
0
e
20
10
0
-10
-20
GI-GS precipitation rate (mm/month)
f
GI-GS precipitation δ18O (‰)
5
4
3
2
1
0
-1
-2
Month

Supplementary information

This file contains a Supplementary Discussion and Supplementary References.

Supplementary Discussion

Climate model simulation

To help evaluate the most plausible factors driving the abrupt decreases of $\delta^{18}O$ in our record, the global rainfall isotopes were simulated for DO event 1/Greenland interstadial 1 (GI-1, Bølling warming)[1-3] based on the TraCE-21K simulation[4,5] between the late interval of Greenland Stadial 2 (GS-2, ~17.0 ka) to the peak of GI-1 (~14.5 ka)[3] (Methods and Supplementary Table 5). These simulations of DO event 1 were used as their climate states are analogous to other DO events during Last Glacial Period[1], with stronger AMOC and higher atmospheric CO_2 and CH_4 during the peaks of DO events (Greenland interstadials) and weaker AMOC and lower CO_2 and CH_4 during the Greenland Stadials prior to the DO events[6-9]. We note there are variations of the sizes of Northern Hemisphere ice sheets between DO event 1 and other DO events, but the uncertainties of ice sheet reconstructions during the last glacial period prevent us from making definitive investigations. Previous studies have demonstrate that the TraCE-21K simulation exhibit reasonable agreements with the data reconstructions of transient evolution of surface temperature over Greenland, sea surface temperature from both Northern and Southern Hemisphere and tropical rainfall between GS-2 to the peak of GI-1[4,10-12]. One isotope simulation was run with boundary conditions from the peak of GI-1 in TraCE-21K to simulate global rainfall isotopes during the peaks of DO events, and another with boundary conditions derived from the late interval of GS-2 to simulate global rainfall isotopes during the stadial condition prior to the peaks of DO events. Thus, the differences of simulated global rainfall isotopes from the two simulations provide the best opportunity to evaluate the most plausible factors driving the abrupt decreases of $\delta^{18}O$ in our record in response to the DO events during the Last Glacial Period.

Proxy-system model: ISOLUTION

We used a proxy-system model to test the feasibility and sensitivity of our interpretation that the observed negative excursions in calcite $\delta^{18}O$ ($\delta^{18}O_{calcite}$) represent large increases in temperature given the relative shift in precipitation $\delta^{18}O$ ($\delta^{18}O_{precip}$) suggested by our modeling. We used the proxy-system model ISOLUTION, developed by Deininger and Scholz (2019)[13], that can be used to explore equilibrium and disequilibrium isotope fractionation processes in speleothems. This model can investigate the dependence of $\delta^{18}O_{calcite}$ on the variation of one or multiple cave-specific parameters, such as cave air temperature, drip interval, cave air pCO_2, relative humidity, and wind velocity. The ISOLUTION model is run in MATLAB and requires 9 input parameters:

1. *Fractionation factor (we use Kim and O'neil, 1997)*
2. *Temperature in ℃*
3. *Drip interval (s)*
4. *Drip water pCO_2 (ppm)*
5. *Cave air pCO_2 (ppm)*
6. *Relative humidity (0<h<=1, where 0.9 = 90%)*
7. *Wind velocity inside the cave (m/s)*
8. *Mixing parameter phi (0<phi<=1)*
9. $\delta^{18}O$ *value of drip water (*‰, which we equate to $\delta^{18}O_{precip}$)

From these input parameters, ISOLUTION calculates modeled $\delta^{18}O_{calcite}$ values.

Model Experiments: Inputs

Cave of the Mounds was a completely closed cave system prior to the 1930s. It is also a relatively shallow cave system (overburden of 10-15 meters), and observations indicate that this shallow setting allows for rapid drip response to rain events[14]. Due to its closed-setting and shallow location in the subsurface, we assigned the following parameters to all simulations:

- Drip interval: 300 (seconds)
- Drip water pCO_2: 1000 (ppm)
- Cave air pCO_2: 700 (ppm)
- Relative humidity: 99%
- Wind velocity: 0 m/s
- Mixing parameter: 1

ISOLUTION experimental setup

For our model simulations and experiments, we changed two values to test our hypothesis: 1. Temperature and 2. Drip water $\delta^{18}O$ ($\delta^{18}O_{dw}$). We assume $\delta^{18}O_{dw} = \delta^{18}O_{precip}$ due to the shallow cave setting as discussed above, we use annual amount-weighted average of $\delta^{18}O_{precip}$ from the isoCAM3 model to assign the test $\delta^{18}O_{dw}$ values, and we assume cave temperature equals annual average surface temperature. We emphasize that, conservatively, this test is most useful for assessing relative changes in $\delta^{18}O_{calcite}$ inferred from relative changes in our climate model output. In order to demonstrate that the warming over Cave of the Mounds could be much larger than 10°C due to the positive $\delta^{18}O_{precip}$ (from GOM-sourced moisture) during GI, we first ran a "GS" simulation to produce a reference value of $\delta^{18}O_{calcite}$. In **Extended Data Table 6**, we present three "GI" simulations that demonstrate the warming required to overcome the effect of COM-sourced moisture increasing $\delta^{18}O_{precip}$ at our site (by increments of +1‰ from 0 to the modeled value of +2‰) and result in a negative $\delta^{18}O_{calcite}$ excursion of the magnitude we observe in our sample (~2‰). The GI-GS temp column (bolded, below) confirms that warming of 10°C or more could be reflected in the negative $\delta^{18}O_{calcite}$ excursions we observe.

Supplementary References

1. Clement, A. C. & Peterson, L. C. Mechanisms of abrupt climate change of the last glacial period. *Reviews of Geophysics* **46**, (2008).
2. Dansgaard, W. *et al.* Evidence for general instability of past climate from a 250-kyr ice-core record. *Nature* **364**, 218–220 (1993).
3. Rasmussen, S. O. *et al.* A stratigraphic framework for abrupt climatic changes during the Last Glacial period based on three synchronized Greenland ice-core records: refining and extending the INTIMATE event stratigraphy. *Quaternary Science Reviews* **106**, 14–28 (2014).
4. Liu, Z. *et al.* Transient simulation of last deglaciation with a new mechanism for Bølling-Allerød warming. *Science* **325**, 310–314 (2009).
5. He, F. *Simulating transient climate evolution of the last deglaciation with CCSM 3*. vol. 72 (2011).
6. Blunier, T. & Brook, E. J. Timing of millennial-scale climate change in Antarctica and Greenland during the last glacial period. *Science* **291**, 109–112 (2001).
7. McManus, J. F., Francois, R., Gherardi, J.-M., Keigwin, L. D. & Brown-Leger, S. Collapse and rapid resumption of Atlantic meridional circulation linked to deglacial climate changes. *Nature* **428**, 834–837 (2004).

8. Ahn, J. & Brook, E. J. Atmospheric CO2 and climate on millennial time scales during the last glacial period. *science* **322**, 83–85 (2008).
9. Henry, L. G. *et al.* North Atlantic ocean circulation and abrupt climate change during the last glaciation. *Science* **353**, 470–474 (2016).
10. He, F. *et al.* Northern Hemisphere forcing of Southern Hemisphere climate during the last deglaciation. *Nature* **494**, 81–85 (2013).
11. Buizert, C. *et al.* Greenland temperature response to climate forcing during the last deglaciation. *Science* **345**, 1177–1180 (2014).
12. He, F. & Clark, P.U., Freshwater forcing of the Atlantic meridional overturning circulation revisited. *Nature Climate Change,* **12,** 449-454 (2022).
13. Deininger, Michael, and Denis Scholz. "ISOLUTION 1.0: an isotope evolution model describing the stable oxygen ($\delta^{18}O$) and carbon ($\delta^{13}C$) isotope values of speleothems." *International Journal of Speleology* 48.1 (2019): 3.
14. Batchelor, C. J., Marcott, S. A., Orland, I. J. & Kitajima, K. Late Holocene increase of winter precipitation in mid-continental North America from a seasonally resolved speleothem record. *Geology* (2022).

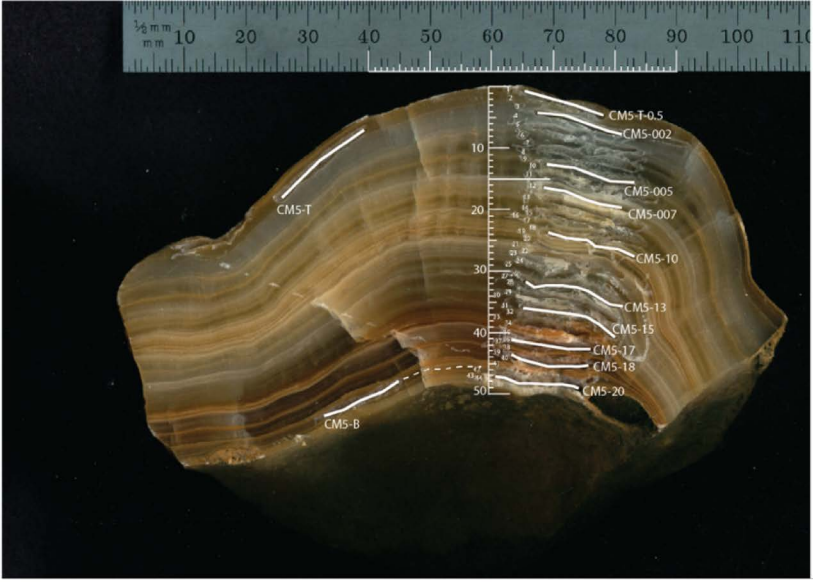
CM5-T-0.5
CM5-002
CM5-005
CM5-007
CM5-10
CM5-13
CM5-15
CM5-17
CM5-18
CM5-20
CM5-T
CM5-B

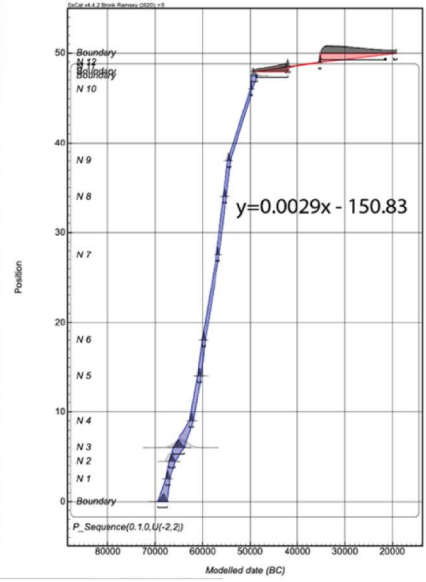
OxCal v4.4.2 Bronk Ramsey (2020); r:5
Boundary
N 12
N 11
N 10
N 9
N 8
N 7
N 6
N 5
N 4
N 3
N 2
N 1
Boundary
y=0.0029x - 150.83
P_Sequence(0.1,0,U(-2,2))
Position
Modelled date (BC)

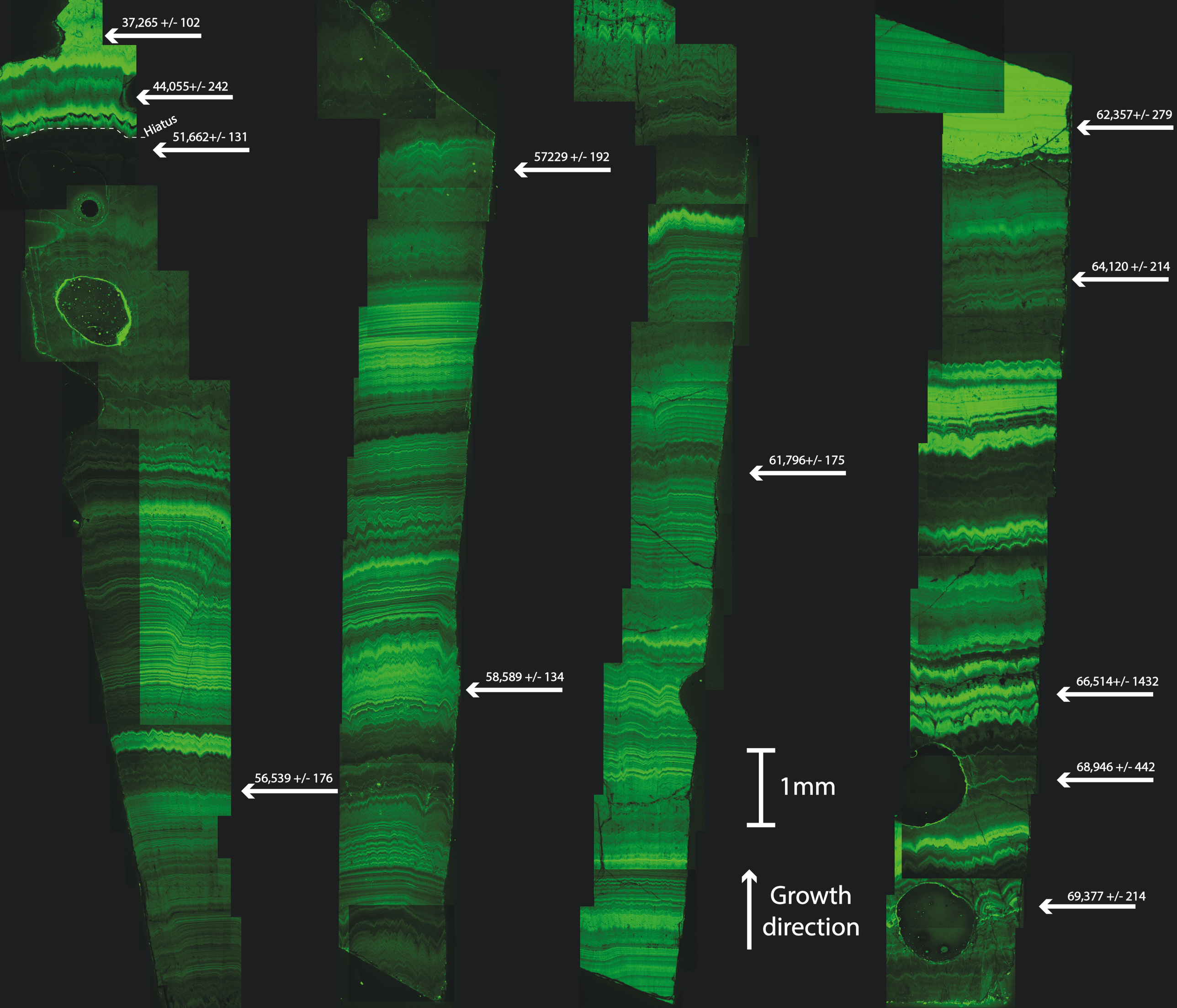
37,265 +/- 102
44,055+/- 242
Hiatus
51,662+/- 131
57229 +/- 192
62,357+/- 279
64,120 +/- 214
61,796+/- 175
58,589 +/- 134
56,539 +/- 176
66,514+/- 1432
68,946 +/- 442
69,377 +/- 214
1mm
Growth direction

a

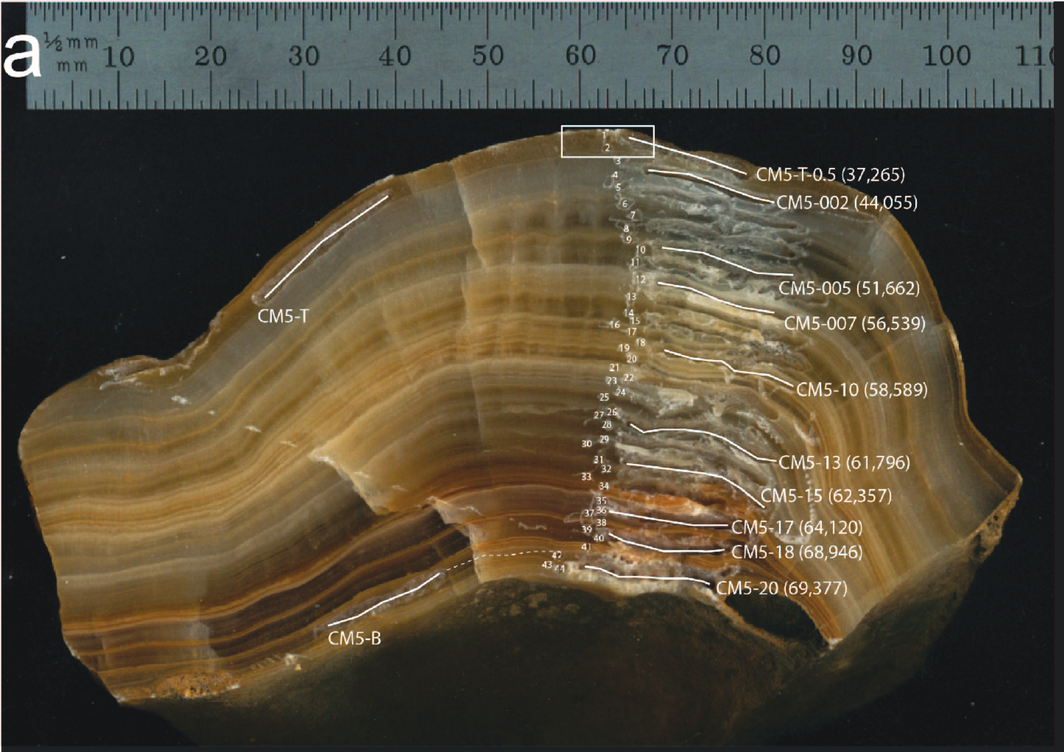
CM5-T
CM5-T-0.5 (37,265)
CM5-002 (44,055)
CM5-005 (51,662)
CM5-007 (56,539)
CM5-10 (58,589)
CM5-13 (61,796)
CM5-15 (62,357)
CM5-17 (64,120)
CM5-18 (68,946)
CM5-20 (69,377)
CM5-B

b

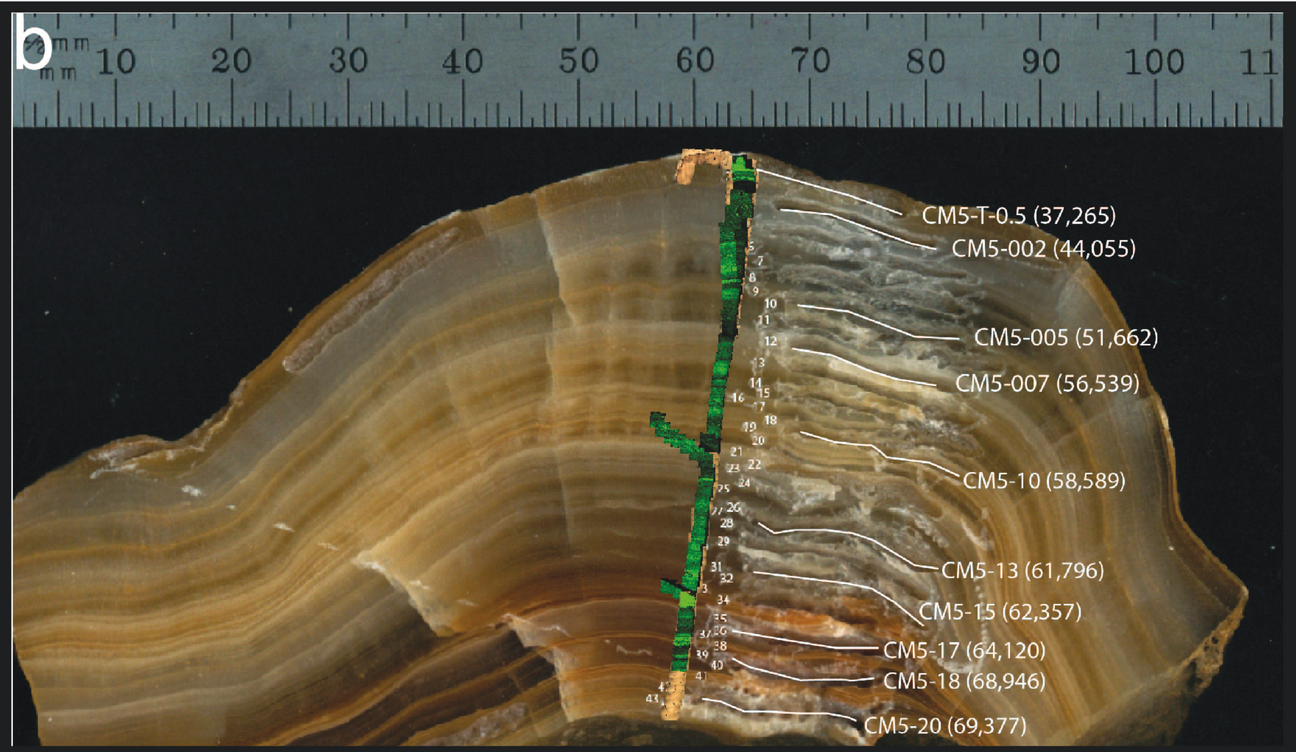
CM5-T-0.5 (37,265)
CM5-002 (44,055)
CM5-005 (51,662)
CM5-007 (56,539)
CM5-10 (58,589)
CM5-13 (61,796)
CM5-15 (62,357)
CM5-17 (64,120)
CM5-18 (68,946)
CM5-20 (69,377)

c

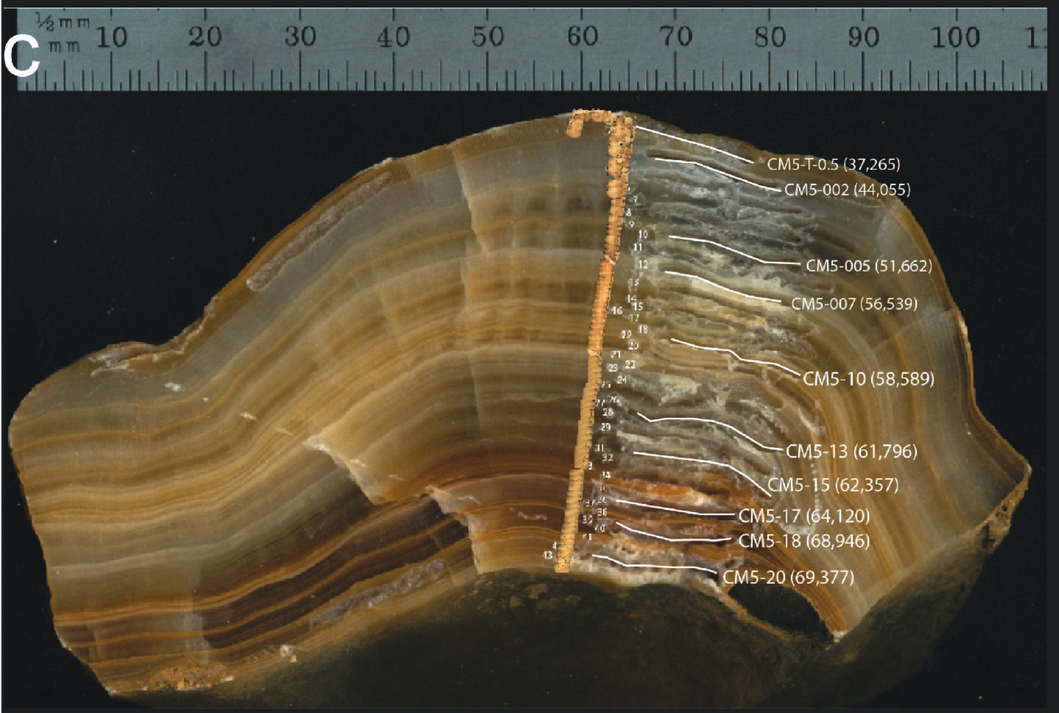
CM5-T-0.5 (37,265)
CM5-002 (44,055)
CM5-005 (51,662)
CM5-007 (56,539)
CM5-10 (58,589)
CM5-13 (61,796)
CM5-15 (62,357)
CM5-17 (64,120)
CM5-18 (68,946)
CM5-20 (69,377)

d

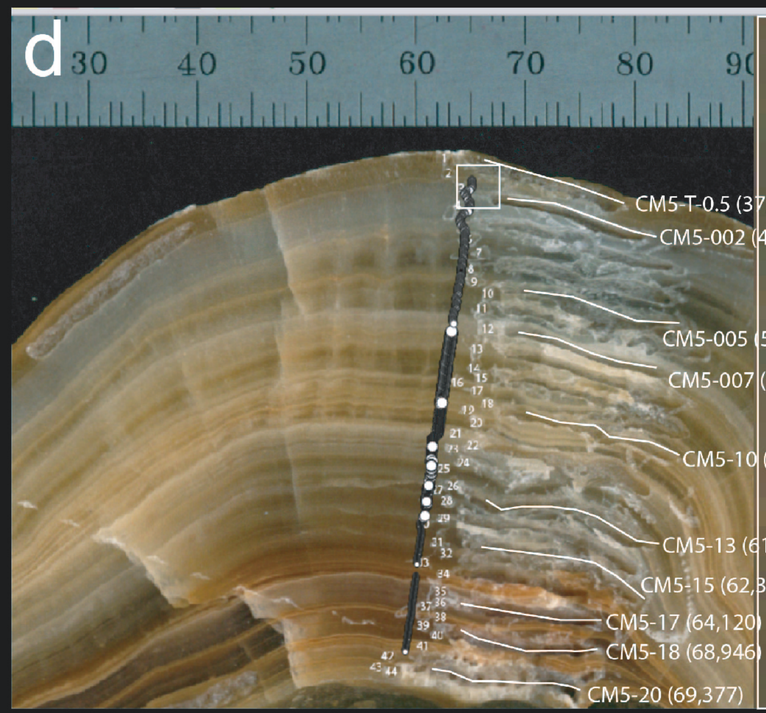
CM5-T-0.5 (37,265)
CM5-002 (44,055)
CM5-005 (51,662)
CM5-007 (56,539)
CM5-10 (58,589)
CM5-13 (61,796)
CM5-15 (62,357)
CM5-17 (64,120)
CM5-18 (68,946)
CM5-20 (69,377)

e

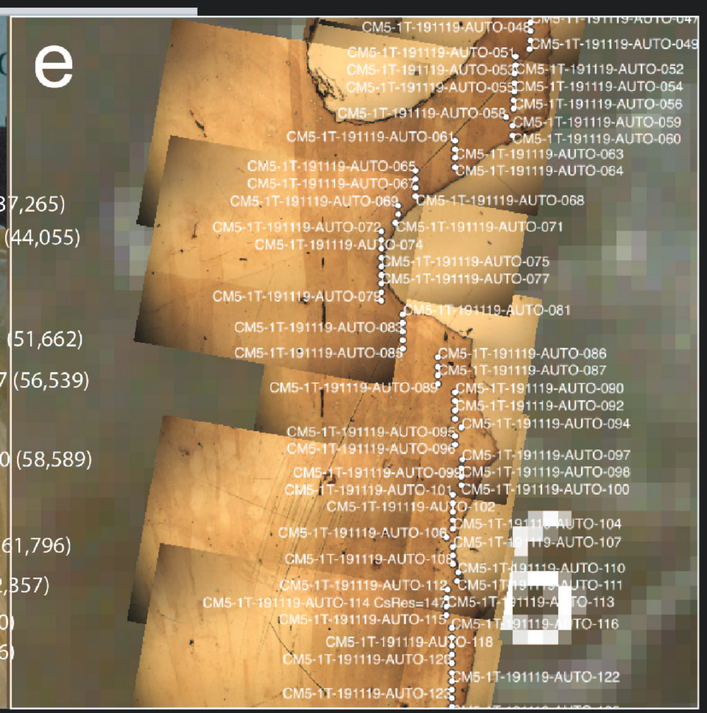
CM5-1T-191119-AUTO-048
CM5-1T-191119-AUTO-049
CM5-1T-191119-AUTO-051
CM5-1T-191119-AUTO-052
CM5-1T-191119-AUTO-053
CM5-1T-191119-AUTO-054
CM5-1T-191119-AUTO-055
CM5-1T-191119-AUTO-056
CM5-1T-191119-AUTO-058
CM5-1T-191119-AUTO-059
CM5-1T-191119-AUTO-060
CM5-1T-191119-AUTO-061
CM5-1T-191119-AUTO-063
CM5-1T-191119-AUTO-064
CM5-1T-191119-AUTO-065
CM5-1T-191119-AUTO-067
CM5-1T-191119-AUTO-068
CM5-1T-191119-AUTO-071
CM5-1T-191119-AUTO-074
CM5-1T-191119-AUTO-075
CM5-1T-191119-AUTO-077
CM5-1T-191119-AUTO-081
CM5-1T-191119-AUTO-086
CM5-1T-191119-AUTO-087
CM5-1T-191119-AUTO-090
CM5-1T-191119-AUTO-092
CM5-1T-191119-AUTO-094
CM5-1T-191119-AUTO-097
CM5-1T-191119-AUTO-098
CM5-1T-191119-AUTO-100
CM5-1T-191119-AUTO-102
CM5-1T-191119-AUTO-104
CM5-1T-191119-AUTO-107
CM5-1T-191119-AUTO-110
CM5-1T-191119-AUTO-111
CM5-1T-191119-AUTO-113
CM5-1T-191119-AUTO-116
CM5-1T-191119-AUTO-118
CM5-1T-191119-AUTO-122

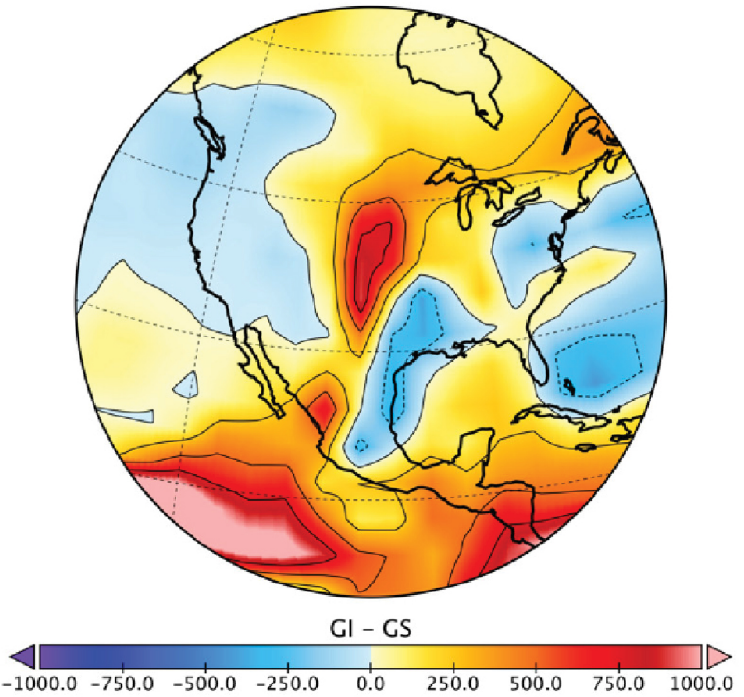
GI – GS
-1000.0 -750.0 -500.0 -250.0 0.0 250.0 500.0 750.0 1000.0

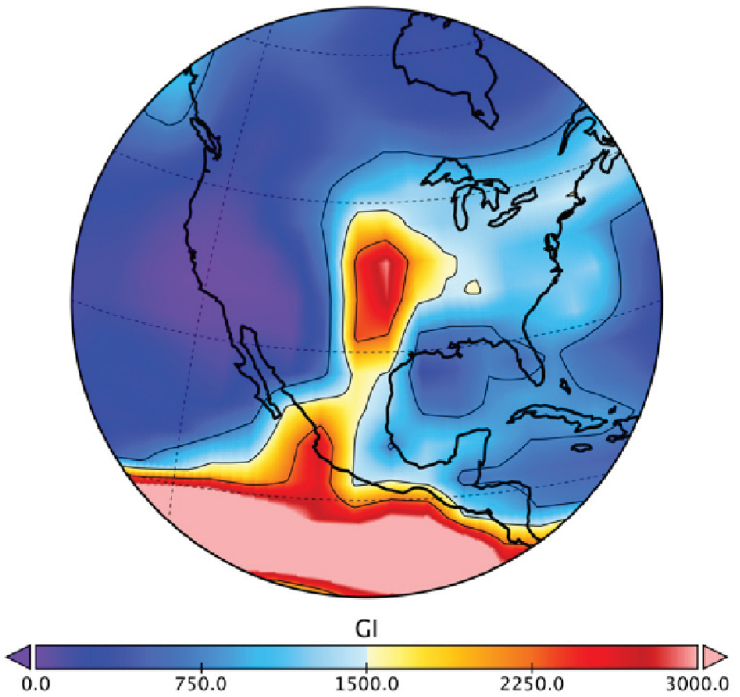
GI
0.0 750.0 1500.0 2250.0 3000.0

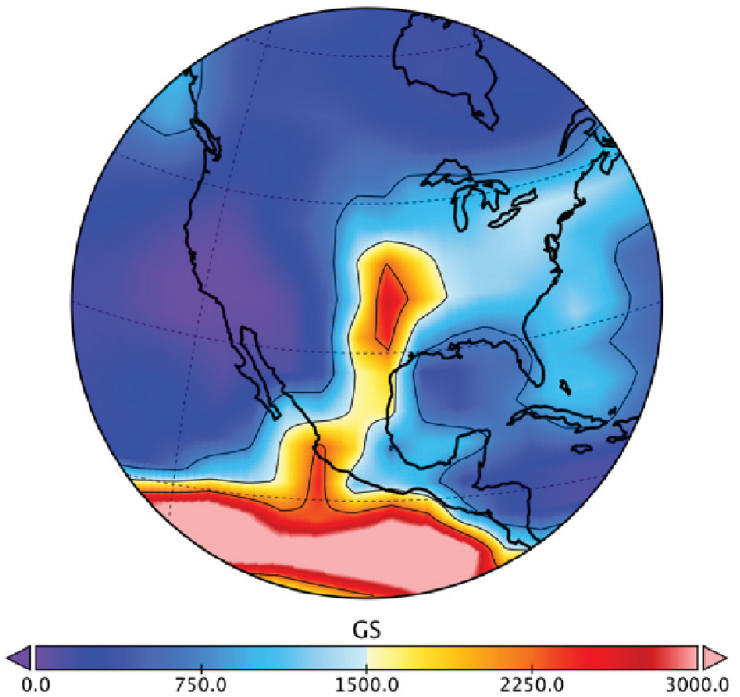
GS
0.0 750.0 1500.0 2250.0 3000.0

GI

Surf Temp (radiative) mean= 283.25 K

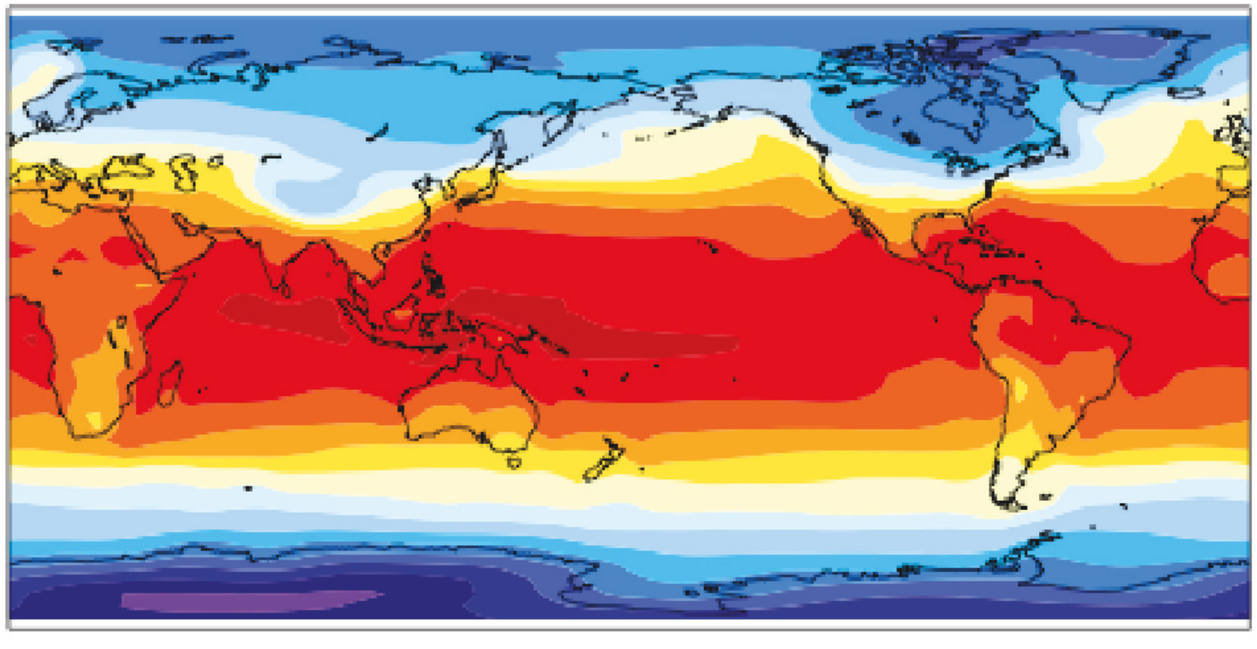

Min = 206.88 Max = 301.22

GS

Surf Temp (radiative) mean= 280.44 K

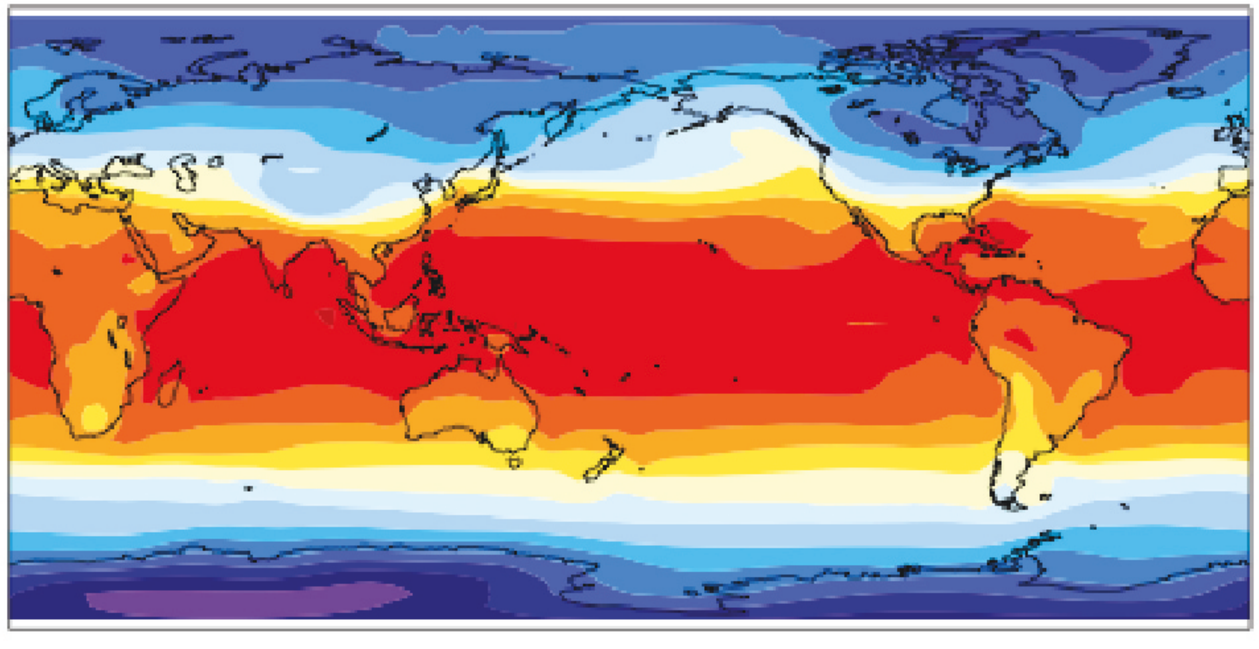

Min = 204.43 Max = 300.39

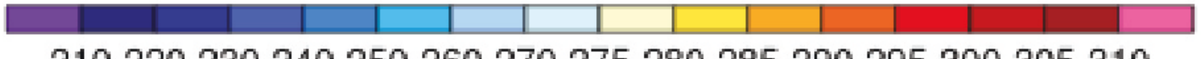

GI - GS

mean = 2.81 rmse = 4.66 K

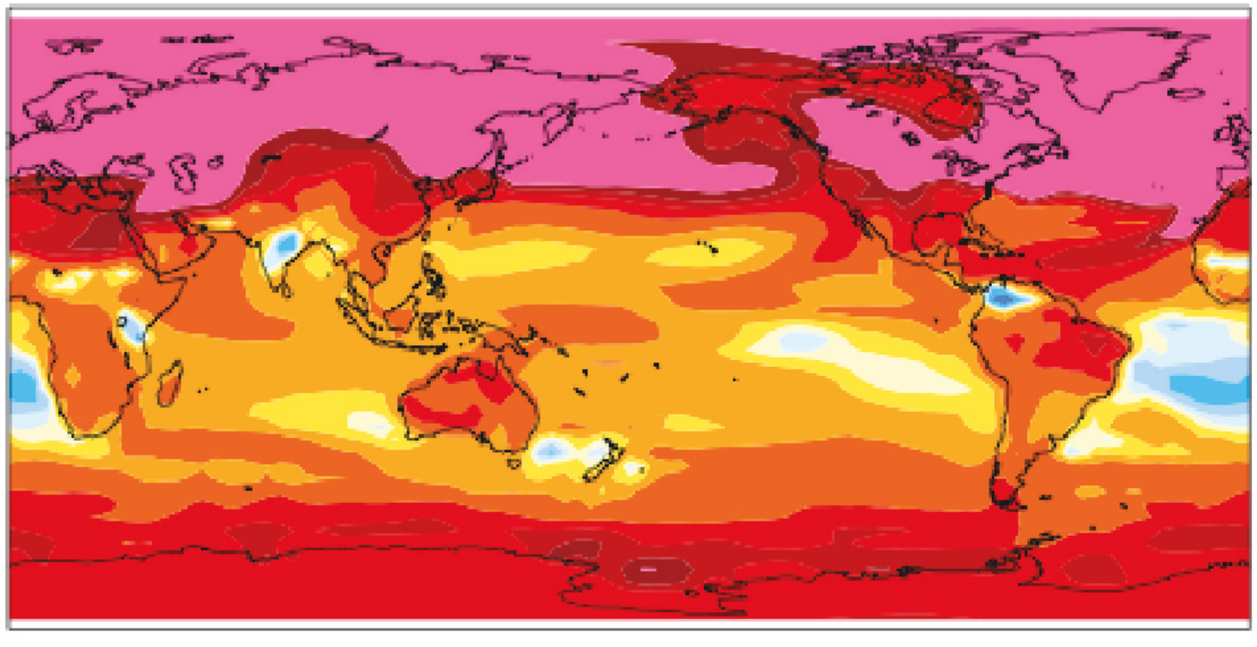

Min = -2.05 Max = 28.65

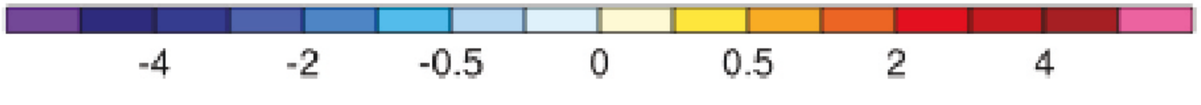

T-test of the two means at each grid point

Colored cells are significant at the 0.05 level

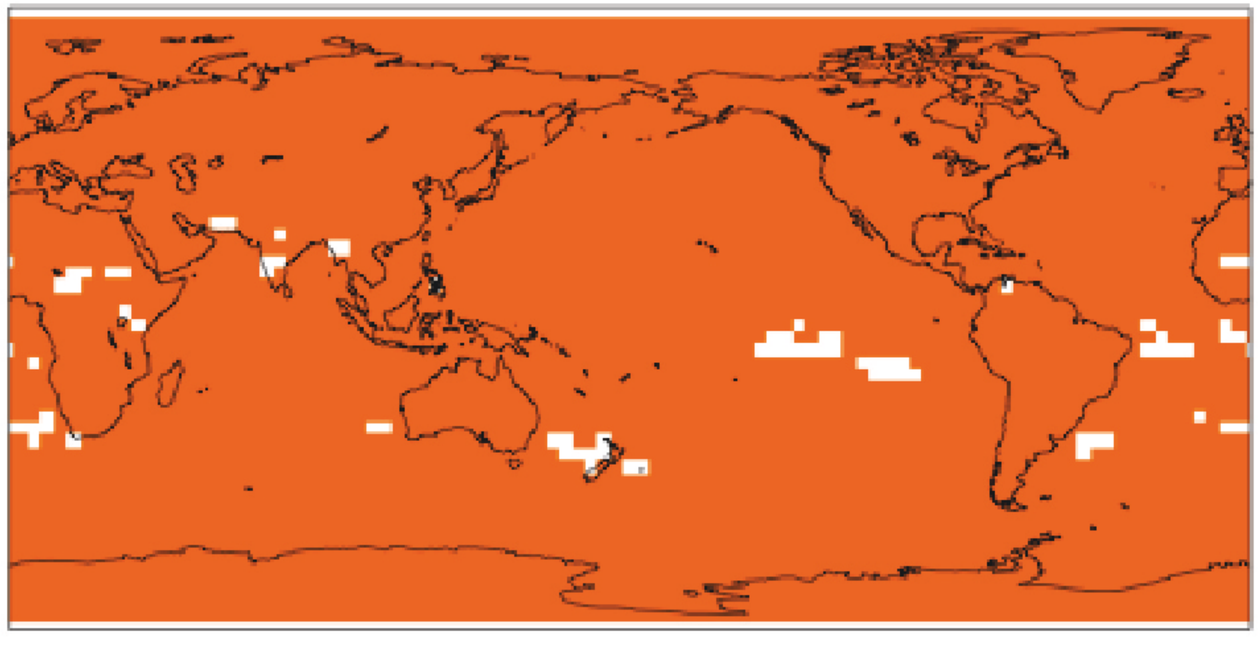

Simulation type	Drip interval (s)	Temp (°C)	Drip water pCO_2 (ppm)	Cave air pCO_2 (ppm)	Relative humidity (%)	Wind velocity (m/s)	Mixing parameter	$\delta^{18}O$ (precip, ‰, VSMOW)	$\delta^{18}O$ (calcite, ‰, VPDB)	GI-GS temp (°C)	GI-GS $\delta^{18}O$ (calcite, ‰, VPDB)
GS	300	5	1000	700	99	0	1	-9	-7.06	-	-
GI (+0‰)	300	10	1000	700	99	0	1	-9	-9.28	**10**	**-2.22**
GI (+1‰)	300	15	1000	700	99	0	1	-8	-9.34	**15**	**-2.28**
GI (+2‰)	300	20	1000	700	99	0	1	-7	-9.36	**20**	**-2.30**